Author contributions
Conceptualization and design of the work: OTQ, CD, EG, and ES. Methodology and performance: OTQ, CD and SS. Data analysis: OTQ, CD. Writing original draft: OTQ. All the authors have revised and edited the manuscript. All authors have read and agreed on the final version of the manuscript.

Conflicts of interest
The authors declare that there are no conflicts of interest.

Data availability
Original files are available Open Access at Zenodo repository:
10.5281/zenodo.6402435

Human Plasma-Like Media fine-tune mitochondrial function and alter drug sensitivity in cancer cell lines

Omar Torres-Quesada[1,2*], Carolina Doerrier[3], Sophie Strich[1], Erich Gnaiger[3], Eduard Stefan[1,2*]

1 Tyrolean Cancer Research Institute, Innrain 66, 6020 Innsbruck, Austria
2 Institute of Biochemistry and Center for Molecular Biosciences, University of Innsbruck, Innrain 80/82, 6020 Innsbruck, Austria
3 Oroboros Instruments, Schoepfstrasse 18, A-6020 Innsbruck, Austria
* Corresponding authors: omar.torres@tkfi.at ; Tel 0043 512 570 48517 / eduard.stefan@uibk.ac.at ; Tel 0043 512 507 57531

Abstract
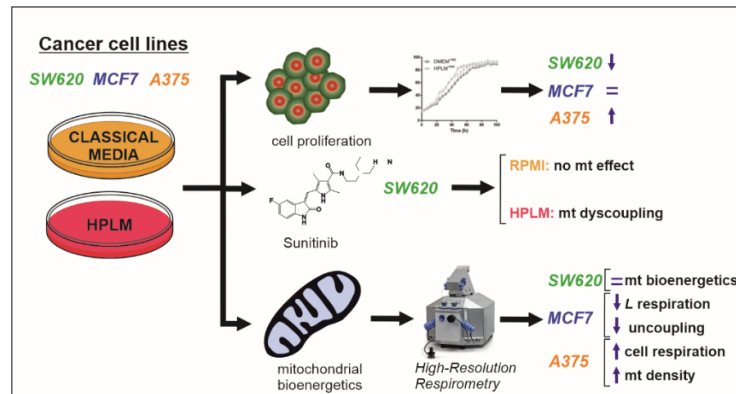
Two-dimensional cell cultures are established models in research for studying and perturbing cell-type specific functions. The simplicity of these models facilitates the reproducible manipulation of cultured cells. Limitations, however, relate to cell growth in a monolayer using standard cell culture media. Although such media are in use for decades, their formulations do not mimic the composition of the originating human cell environment in physiological or pathological conditions. In this study, we selected three frequently-used cancer cell lines SW620 (colon cancer), MCF7 (breast cancer), and A375 (melanoma)

residual O_2 consumption; bioenergetic cluster analysis BCA

to determine the impact of a newly formulated human plasma-like medium (HPLM) on cell proliferation and mitochondrial function. Mitochondrial bioenergetic profiles were analyzed by high-resolution respirometry, revealing metabolic reprogramming in cells cultured in standard and HPLM media. Notably, the culturing of differentially proliferating cells in HPLM affected key mechanism of cellular respiration. All three cancer cell lines displayed an amending bioenergetic profile, particularly related to mitochondrial density and mild uncoupling of respiration. Importantly, only cells cultured in HPLM displayed mitochondrial dysfunction upon exposure with the clinically prescribed cancer drug and kinase inhibitor sunitinib. These findings highlight that cell culture media redirect mitochondrial function and affect cancer drug sensitivities. To advance the translational potential of cell culture models we propose to prioritize media with a human plasma-like composition for analyzing bioenergetic profiles and for determining target-oriented drug efficacies.

1. Introduction

Diverse cell culture models are commonly used to study the etiology and progression of a defined cancer cell population originating from patient specimens. Two-dimensional cell cultures (2D) provide standardized models suitable for reproducible drug screening and determination of drug efficacy by ensuring the accessibility of the experimental lead molecule to the cell monolayer. However, the artificial set-up for culturing cells is limited due to the lack of various physiological components, metabolites and factors which are trackable e.g. in the human plasma or in the tumor microenvironment (Kapalczynska et al 2018). It is thus an acute challenge to develop and advance media formulations with a more human like (patho)physiological composition.

The selection of the growth medium influences the metabolism and thus cell growth in culture. In addition, the nutrient composition of the culture medium affects distinct cell-type specific features of the cell (Morgan et al 1950). This involves the exposure to diverse environmental stimuli for redirecting signaling events and gene expression signatures. Classical cell culture media should hold the promise to create the growth conditions for the *in vitro* cell lines. However, usually these formulations do not mimic the physiological conditions or the composition of the tumor microenvironment. Among the most frequently used cell culture media are Eagle's Minimal Essential Medium (MEM), its Dulbecco's modified version (DMEM), and RPMI 1640 (Eagle, 1955, Eagle, 1959, Moore et al 1967). They were designed to support continuous growth of cancer cells. However, the composition and concentrations of several metabolites, including glucose and amino acids, do not reflect the molecular composition of human plasma. Recently two new formulations of cell culture media have been developed; Human Plasma-like Medium (HPLM, Thermofisher) and the similar Plasmax™ (Ximbio) were established as alternatives to classical cell culture media (Cantor et al 2017; Vande Voorde et al 2019).

HPLM contains a cocktail of 31 physiological components that are absent in commonly used cell culture media. Further, HPLM contains physiologically relevant concentrations of a collection of typical media components such as glucose, amino acids, and electrolytes (Cantor et al 2017). Importantly, cells grown in HPLM compared to classical media formulations have different cellular signatures which are related to adaptions of the metabolome, redox state, *de-novo* pyrimidine synthesis pathway, and lipid peroxidation and ferroptosis (Cantor et al 2017; Leney-Greene et al 2020; Vande Voorde et al 2019). HPLM induces changes in gene expression of human essential genes (Rossiter et al 2021).

Mitochondrial metabolism is linked to different stages of carcinogenesis (Parri et al 2020). Mitochondria act as dynamic cell organelles by orchestrating the cellular energy transformation. Besides being the bioenergetic powerhouse of the cell, mitochondria play a crucial role in many central cellular processes such as biosynthesis, calcium and lipid homeostasis, cell division, and apoptosis (Moreno-Sanchez et al 2010; Rinaldi et al 2018). The metabolic reprogramming of cancer cells is sustained by the accessibility of nutrients and secondary intracellular alterations and adaptions of signaling events. Indeed, environmental conditions in cell culture models impact potencies and efficacies of intervention strategies (Moretto et al 2011; Sams-Dodd 2005). This variability of ill-defined cell culture conditions may contribute to discrepancies of *in vivo* and *in vitro* studies focusing on mitochondrial bioenergetics and off-target drug effects (Nadanaciva et al 2009; Schopf et al 2016).

Here, we set out to determine the precise impact of cell culture media compositions on cell proliferation and mitochondrial function. To determine mitochondrial bioenergetic profiles of several standard cancer cell lines, we used high-resolution respirometry (HRR) for quantitative evaluation of cell respiration (Gnaiger 2020). Furthermore, we evaluated whether HPLM influences mitochondrial drug sensitivity in cells exposed to the tyrosine kinase inhibitor sunitinib. The newly formulated HPLM had distinct effects on cell proliferation and mitochondrial respiration under steady-state conditions and after exposure to sunitinib when compared to classical cell culture media. Overall, this study highlights the necessity to evaluate the choice of cell culture media for studying pharmacological targeting of key events of metabolic and pathophysiological functions.

2. Materials and methods

2.1. Cell culture

The human cancer cell lines were purchased from ATCC (Manassas, Virginia): SW620 (ATCC® CCL-227™, metastatic-derived colon cancer), the MCF7 (ATCC® HTB-22™, breast cancer) and A375 (ATCC® CRL-1619™, malignant melanoma). Cells were incubated at 37 °C in a humidified incubator with 5 % CO_2 in air. For the SW620 and MCF7 cell lines, we generated a RPMI formulation with physiological glucose concentration (5 mM) supplemented with 10 % dialyzed fetal bovine serum (FBS) (PAN BIOTECH, P30-2102). For the A375, we generated a DMEM with 5 mM glucose supplemented with 10 % dialyzed FBS. The new HPLM (Thermo Fisher Scientific, A4899101) was supplemented with 10 % dialyzed FBS. Cells were counted in a Cellometer® counter (Nexcellon Bioscience, Lawrence, Massachusetts) following the manufacturer's instructions. Briefly, a 100 μL aliquot of the cells was diluted in 0.1 % trypan blue and measured in a Cellometer® chamber.

For the sunitinib treatments, SW620 cells were cultured either in RPMI or HPLM supplemented with 10 % dialyzed FBS. At the day of the experiment, cells were treated for 3 h with 10 μM sunitinib (MedChemExpress, HY-10255A) dissolved in DMSO. After the incubation period, the cells were washed with PBS, detached with trypsin EDTA, counted, and subjected to respirometry.

2.2. Proliferation assays

For the proliferation studies, cells were seeded in a 96-well plate format (Corning) with a density of 10 000 cells/well. Cell growth was monitored during 100 h with scanning points every 4 h in an Incucyte® S3 Live-Cell Analysis System (Essen Bioscience, Royston, United Kingdom). Phase-area confluency was calculated using the Incucyte® analysis software. Area-under-the curve (AUC) and marginal distribution (slope variation) were performed using the software GraphPad Prims 6.

2.3. Sample preparation and high-resolution respirometry

Prior to the respirometric measurements, SW620 and MCF7 cell populations were grown for four days in RPMI^{+FBS} and HPLM^{+FBS}; A375 cells were grown in DMEM^{+FBS} and HPLM^{+FBS}. Next, cells were trypsinized and resuspended in the corresponding cell culture media at a cell concentration of approximately $1.0 \cdot 10^6$ x/mL for SW620 and A375 and $0.7 \cdot 10^6$ x/mL for MCF7. In case of cells exposed to sunitinib, $1.0 \cdot 10^6$ x/mL SW620 cells were suspended in the cell media containing the same concentration of solvent or inhibitor used for the treatments. The elementary entity "x" represents the single individual cell (Gnaiger 2020).

O_2 consumption in living cells was measured using the O2k-FluoRespirometer (O2k, Oroboros Instruments, Innsbruck, Austria), a modular system for HRR. Temperature was maintained constant at 37 °C ± 0.002 °C (electronic Peltier temperature control) under constant stirring at 750 rpm, which ensured a homogenous O_2 concentration in the experimental closed chambers with experimental volumes of 2 mL. O_2 concentration c_{O2} [μM] and O_2 flow per cell I_{O2} [amol·s^{-1}·x^{-1}] (Gnaiger 2020) were monitored real-time using DatLab 7.4 software (Oroboros Instruments, Innsbruck, Austria). Calibrations of the polarographic O_2 sensors of the O2k were performed daily, using an O_2 solubility factor relative to pure water of 0.89 as in serum (Gnaiger 2008) and correcting the partial O_2 pressure for barometric pressure monitored by the O2k. Instrumental O_2 background tests were performed at monthly intervals (Doerrier et al 2018). The coupling control protocol for living cells (SUIT-003 D009) was applied which allows the study of the different coupling control states in living cells: ROUTINE, LEAK and electron-transfer pathway capacity (Gnaiger 2020). Cell addition into the O2k chambers was performed by complete volume replacement of the sample. ROUTINE respiration R is a physiological coupling state in which respiration is controlled by aerobic ATP demand. This step was followed by the inhibition of the phosphorylation system with oligomycin (Omy) which induces LEAK respiration L. The inhibitory concentration of 10 nM was tested for each cell line. Subsequently, the protonmotive force was dissipated by stepwise titration (0.5 μM/step) of the uncoupler U carbonyl cyanide 3-chlorophenylhydrazone (CCCP) until the maximum noncoupled respiration was obtained (ET capacity E). The addition of 0.5 μM rotenone (Rot) and 5 μM antimycin A (Ama) inhibited the ET pathway, allowing the measurement of residual oxygen consumption Rox. Data analysis was performed using

DatLab 7.4. Respiratory rates were corrected for the instrumental O_2 background flux, dilution of the sample by titrations, and *Rox*.

To provide respiratory control fingerprints of coupling control, flux control ratios *FCR*, coupling-control ratios and flux control efficiencies were calculated. *FCR* provide normalizations of O_2 flow in any respiratory state (*i*) of a SUIT protocol by an internal functional mitochondrial marker. *FCR* are independent of cell count, cell size and mitochondrial density (Gnaiger 2020),

$$FCR = \frac{I_{O_2}(\text{state } i)}{I_{O_2}(\text{reference state})}$$

ET capacity *E* was measured as the maximum respiration obtained in uncoupler titrations and defined as the common reference state. Additionally, *L/R* coupling-control ratios, *E-L* net ET capacities, net *R/E* control ratios, *E-L* coupling efficiencies, and *R-L* coupling efficiencies were calculated (Gnaiger 2020; Gnaiger 2021).

2.4. Statistical analysis

Statistical significance levels *p* were assessed using the non-parametric unpaired Mann-Whitney t-test. For multiple comparisons (respiratory control coupling states) a two-way ANOVA with Bonferroni´s multiple comparison test was used. Statistical analyses were performed using the software GraphPad Prims 6.

3. Results

3.1. HPLM influences steady state cancer cell proliferation and mitochondrial function.

We selected several human cancer cell lines from different human tissues displaying different phenotypic features (cell size and morphology) and a different mutational burden.

To assess the impact of HPLM on key features of the SW620, MCF7, and A375 cancer cell lines we compared the proliferation profiles of cell populations cultured in classical media and the new HPLM (denoted as RPMI+FBS, DMEM+FBS and HPLM+FBS). The differences of formulations between RPMI, DMEM, and HPLM are summarized in Figure 1.
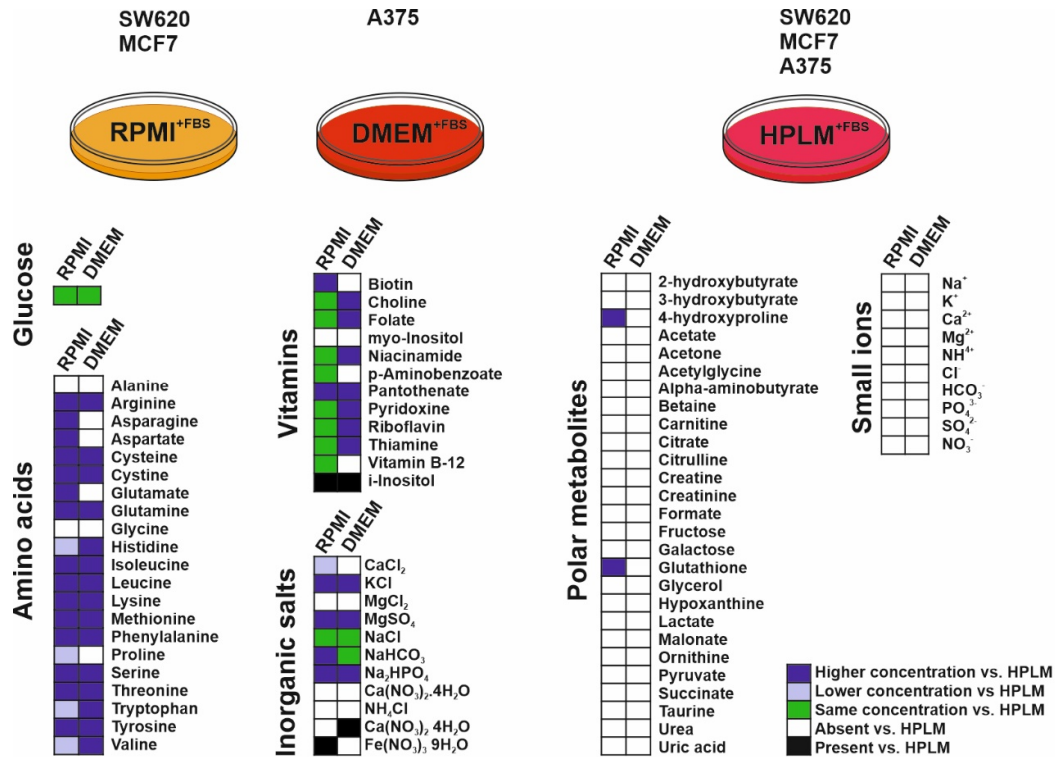
Figure 1. Media formulation of RPMI, DMEM, and HPLM. All experiments were performed in these media supplemented by 10 % FBS. The chart shows the relative concentrations of RPMI and DMEM media supplemented with 5 mM glucose compared with HPLM (Cantor et al 2017). Components not present in RPMI and DMEM but present in HPLM are denoted as "absent"; components not present in the HPLM but present in the other media are denoted as "present".

First, we tracked cell proliferation kinetics in terms of confluence as a function of time and the proliferation rates as the area under the curve AUC. Linear regressions of these data sets highlight differences of growth curves for two cell lines. The proliferation rate in SW620 cells cultured in HPLM+FBS was decreased, starting at 40 h and causing a difference of 29.5 h. This led to a strong delay of SW620 growth in HPLM+FBS (Figure 2a-c). Differences in MCF7 proliferation were undetectable (Figure 2d-f). In contrast, the proliferation rates were augmented in the melanoma cell line A375 in the presence of HPLM+FBS (Figure 2g-i). Taken together, HPLM supported growth of all three cell lines. However, HPLM+FBS surprisingly exerted opposite effects on cancer cell proliferation of SW620 and A375 cell lines.
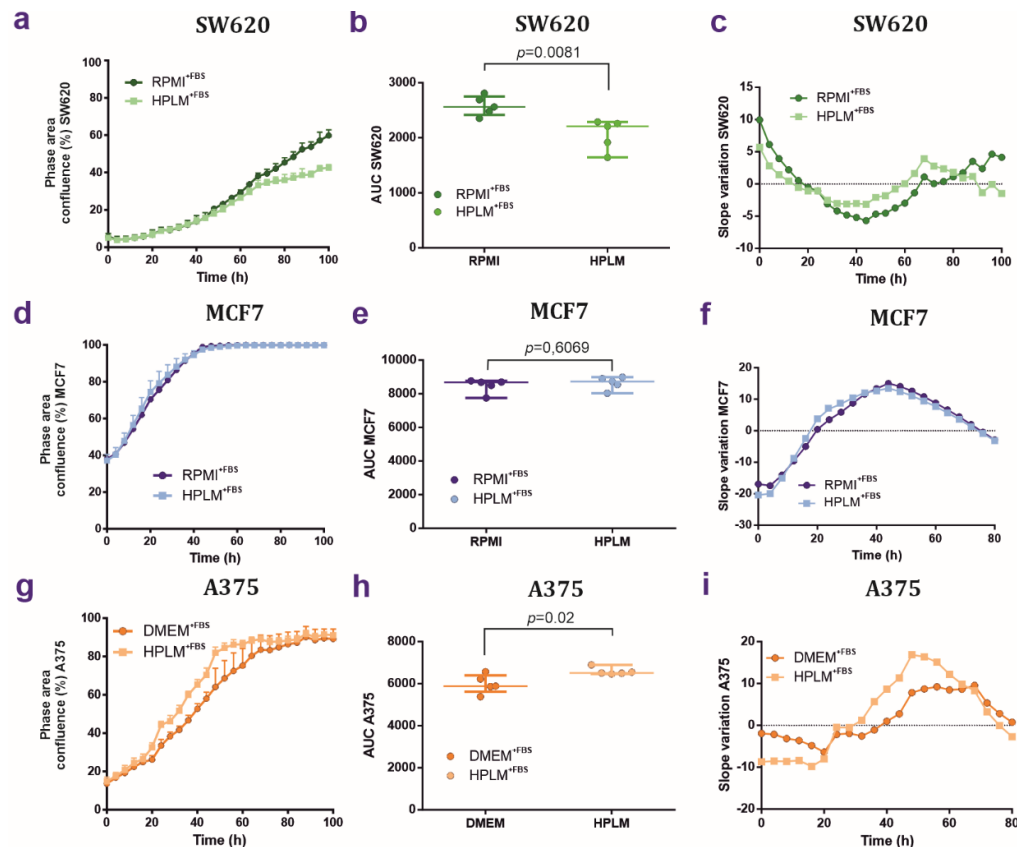
Figure 2. Effect of HPLM on cell growth of SW620, MCF7, and A375 cell lines. **(a-c)** Proliferation of SW620 cells grown in RPMI^{+FBS} or HPLM^{+FBS}. Grown curves are shown in **(a)**, AUC are plotted in **(b),** and slope variations are shown in **(c)**. **(d-f)** Same analyses performed for MCF7 cells grown in either RPMI or HPLM showing proliferation curves **(g),** AUC **(h)** and slope variation **(i). (g-i)** Proliferation of the A375 cell line grown either in DMEM^{+FBS} or HPLM^{+FBS}. In proliferation curves and AUC, values are represented as median ± IQR. Unpaired non-parametric t-test analysis; *N*= 5.

To address if HPLM^{+FBS} affects mitochondrial respiratory control in these cell lines, we measured cell respiration by HRR. Results on cell respiration of living cells are shown in Figure 3. (*1*) HPLM^{+FBS} exerted no detectable effects on cell respiration of the SW620 cell line in the ROUTINE, LEAK and ET states (Figure 3a and b). A higher concentration of the uncoupler CCCP was needed to reach the maximum ET capacity in cells grown in HPLM^{+FBS} compared to RPMI^{+FBS} ([U] = 7.0 ± 1.1 μM for RPMI^{+FBS} versus [U] = 9.5 ± 1.6 μM for HPLM^{+FBS}; Figure 3a). (*2*) ROUTINE respiration and to a bigger extend ET capacity were increased in MCF7 cells grown in HPLM^{+FBS} (Figure 3c and d). (*3*) Respiration in all coupling control states — with major effects on ROUTINE respiration and ET capacity — was increased in A375 melanoma cells cultured in HPLM^{+FBS} compared to DMEM^{+FBS} (Figure 3e and f). Results are summarized in Table S1a.
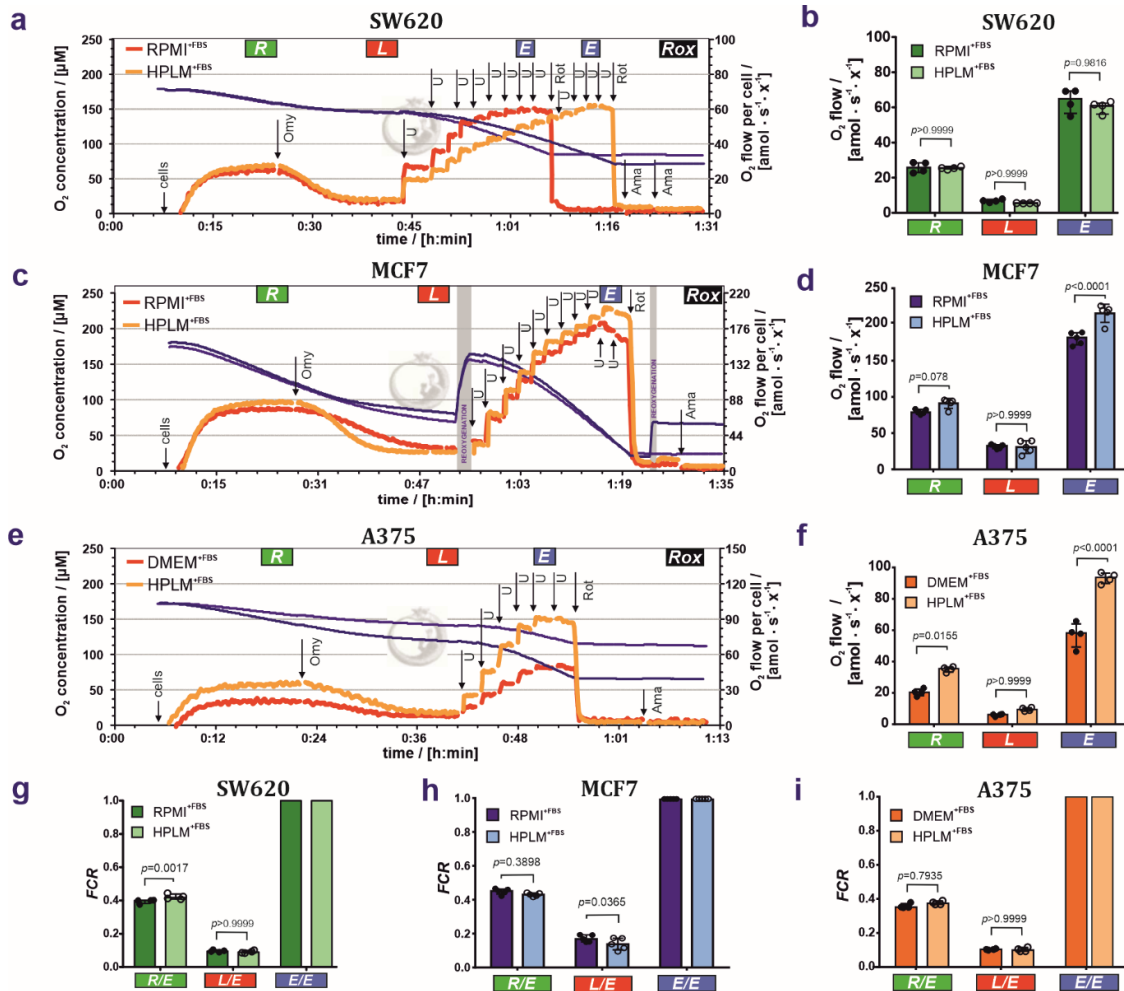
Figure 3. HPLM impacts mitochondrial function in SW620, MCF7, and A375 cell populations when compared to standard cell culture media. (a, **c, e)** Representative respiratory traces for coupling control protocol SUIT-003-D009 in **(a)** SW620, **(c)** MCF7, and **(e)** A375 cells. Blue lines: O_2 concentration [µM], dark orange lines: O_2 flow per cell [amol·s^{-1}·x^{-1}] in cells grown and measured in **(a, c)** RPMI^{+FBS} or **(e)** DMEM^{+FBS}, light orange lines: O_2 flow per cell [amol·s^{-1}·x^{-1}] in cells grown and measured in HPLM^{+FBS}. "x" represents the unit cell. Sequential steps: cell addition (cells), oligomycin (Omy), uncoupler CCCP (U), rotenone (Rot) and antimycin A (Ama). Total ROUTINE respiration (R'_{tot}), LEAK respiration (L'_{tot}), and ET capacity (E'_{tot}) not baseline-corrected for residual O_2 consumption (Rox). **(b**, **d, f)** O_2 flow (R, L, E) [amol·s^{-1}·x^{-1}] baseline-corrected for Rox in **(b)** SW620, **(d)** MCF7 and **(f)** A375 cell lines. **(g-i)** Flux control ratios FCR in SW620, MCF7 and A375 cells lines. Results are represented as median ± IQR (50 % range). 2-way ANOVA with Bonferroni´s multiple comparison test or non-parametric unpaired t-test analysis; N= 4 - 5.

To determine coupling control in these cells we calculated respiratory FCR, coupling-control ratios and flux control efficiencies (Gnaiger 2020) (Figure 3g-i, summarized in Table S1b). First, in the SW620 cell line, the FCR for ROUTINE respiration (R/E, Figure 3g) was slightly increased in HPLM^{+FBS}. Furthermore, we observed in SW620 cells grown in HPLM^{+FBS} a significant reduction of the L/R coupling-control ratio and elevation of the net R/E control ratio and R-L control efficiency (Table S1b) (Gnaiger 2020). ATP demand and

uncoupling or dyscoupling are drivers of ROUTINE respiration in living cells. Consequently, higher R/E may indicate an increase in uncoupling. However, no differences were observed between both media in LEAK respiration (Figure 3b, Table S1a), L/E coupling-control ratio (Figure 3g, Table S1b) and E-L coupling efficiency (Table S1b). Therefore, our findings might reflect that the increase in R/E and R-L control efficiency in cells grown in HPLM[+FBS] is controlled by changes in cellular energy demand and energy turnover compared to RPMI[+FBS]. Additionally, no differences were observed between both media (Figure 4a, b, c, j) when applying bioenergetic cluster analysis (BCA) (Gnaiger 2021; Zdrazilova et al 2022), indicating that the mitochondrial bioenergetic profiles are similar. Second, in MCF7 cells, higher L/E FCR (Figure 3h, Table S1b) and lower E-L coupling efficiency (Table S1b) in RPMI[+FBS] compared to HPLM[+FBS] indicate higher intrinsic uncoupling in cells grown in RPMI[+FBS]. BCA in MCF7 cells identified two clusters in the scatter when LEAK respiration is expressed over ROUTINE respiration (Figure 4d), and ROUTINE respiration (Figure 4e), LEAK respiration (Figure 4f) and E-L coupling efficiency (Figure 4k) are expressed over ET capacity. BCA supports that respiration in MCF7 cells is better coupled when cells are grown in HPLM[+FBS], by showing a drop in E-L coupling efficiency over ET capacity in the cluster RPMI[+FBS] compared to HPLM[+FBS] (Figure 4k). This lower coupling control efficiency in RPMI[+FBS] might be caused by an ET- and uncoupling-linked effect observed in RPMI[+FBS] (Figure 3d and h, Table S1b) (Gnaiger 2021; Zdrazilova et al 2022). Finally, we applied the same analysis to data sets of A375 cells. The FCR showed no difference between DMEM[+FBS] and HPLM[+FBS] (Figure 3i), indicating that the changes in O_2 fluxes might originate from an increase in mitochondrial content and/or density. BCA analysis supports the same observation, with the generation of two isolinear clusters with similar coupling efficiencies (Figure 4g, h, i, l). Interestingly, the A375 cell line showed a reduction of Rox in cells grown in HPLM[+FBS] as compared with DMEM[+FBS] (Table S1b and Figure S1).
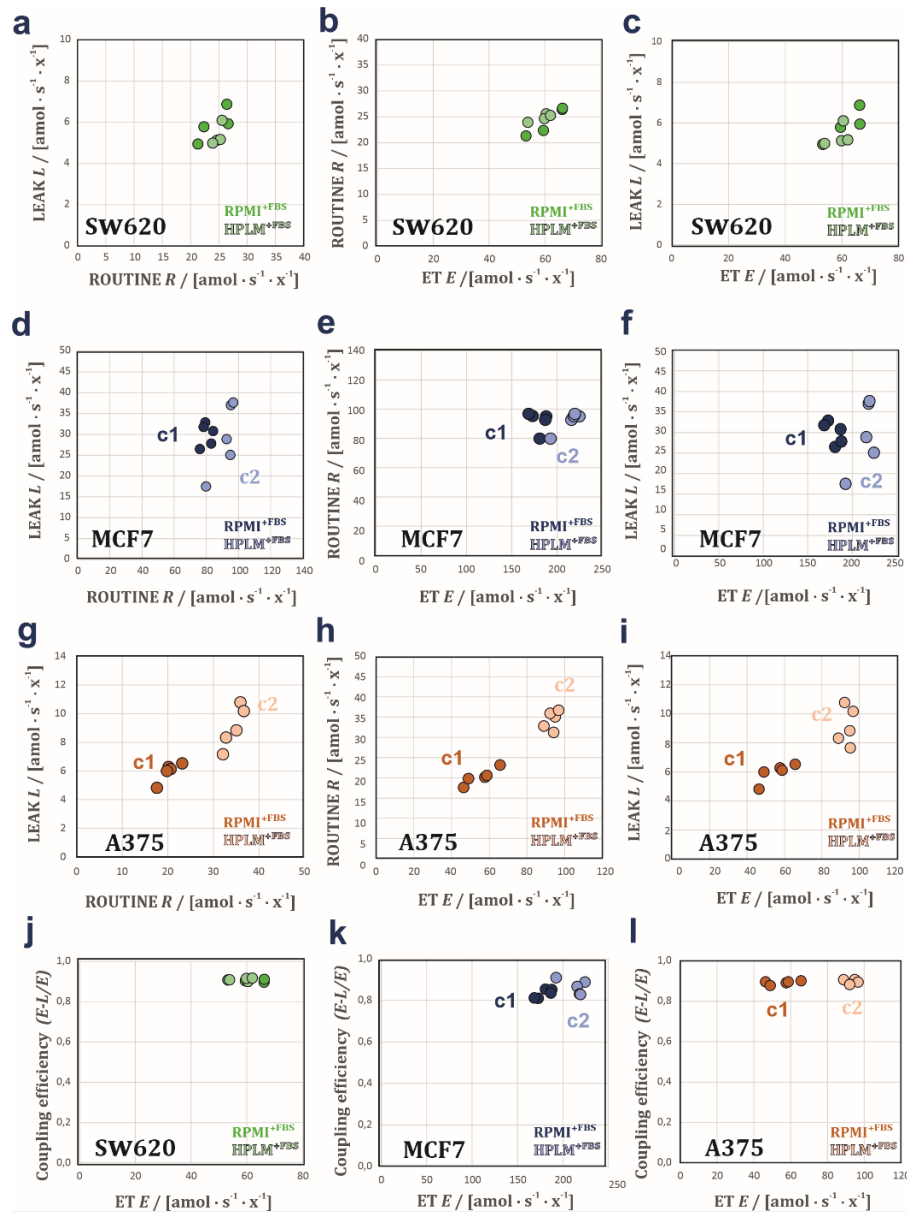
Figure 4. Bioenergetic cluster analysis in different respiratory coupling states of the SW620, MCF7, and A375 cell lines grown in classical and HPLM media. Plots of L over R, R over E, and L over E. **(a-c)** SW620 showing no cluster differences between RPMI and HPLM. **(d-f)** MCF7 showing two heterolinear bioenergetic clusters (Gnaiger 2021) in RPMI (c1) and HPLM (c2). This indicates changes in mitochondrial quality between both media. **(g-i)** A375 showing two isolinear bioenergetic clusters (Gnaiger 2021) in DMEM (c1) and HPLM (c2). Proportionality with zero intercept indicates changes of mitochondrial density in the cells grown in the two media. **(j-l)** Coupling efficiencies (E-L)/E over ET capacities in SW620 **(j)**, MCF7 **(k)** and A375 **(l)**. The lower $(E\text{-}L)/E$ values in MCF7 cells in RPMI at lower ET values indicate a drop in mitochondrial quality with RPMI. In A375, the $(E\text{-}L)/E$ values remain constant over ET in both media indicating that mitochondrial quality is preserved (Gnaiger 2021; Zdrazilova et al 2022).

3.2. HPLM modifies mitochondrial drug sensitivity in cancer cells.

After the characterization of mitochondria in steady-state conditions, we asked whether HPLM influences drug sensitivity in cancer cells. For this purpose, we cultivated the SW620 cells either in RPMI^{+FBS} or HPLM^{+FBS} and then exposed them to the receptor tyrosine kinase inhibitor sunitinib (Sutent, SU11248), which is currently used as a cancer therapy against renal cell carcinoma and gastrointestinal stromal tumor (Chiusa et al 2012; Goodman et al 2007). Following treatments with sunitinib we performed respirometric measurements. First, lower uncoupler concentrations were needed to reach ET capacity E in cells grown in HPLM^{+FBS} and treated with sunitinib (HPLM DMSO: [U] = 11,2 ± 4.5 μM versus HPLM Sunitinib: 9,4 ± 5 μM) in contrast to cells grown in RPMI^{+FBS} (RPMI DMSO: [U] = 5,8 ± 1.5 μM vs RPMI Sunitinib: 5,9 ± 1.75 μM) (Figure 5a-b). Second, in contrast to cells grown in RPMI^{+FBS}, SW620 cells exposed to sunitinib and grown in HPLM^{+FBS} showed a decrease in the ET capacity (Figure 5c-g, Table S2a).
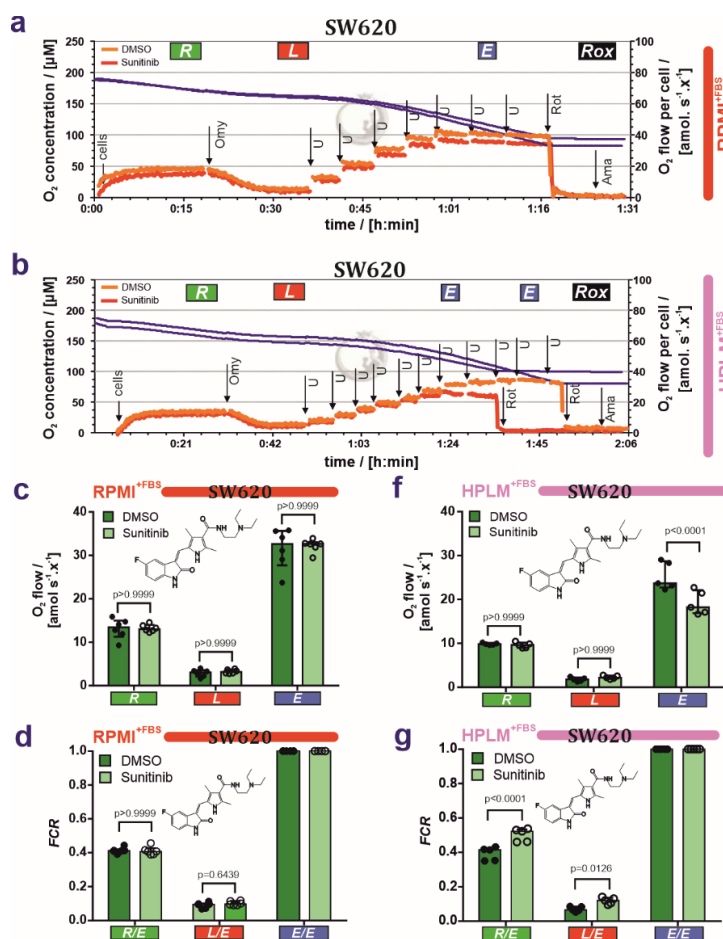

Figure 5. HPLM influences sunitinib effect on cell respiration in SW620 cells. (a - b) Representative respiratory traces for coupling control protocol SUIT-003-D009 in SW620 cells grown in **(a)** RPMI^{+FBS} and **(b)** HPLM^{+FBS}, and exposed to 10 μM sunitinib for 3 hours. Blue lines: O$_2$ concentration [μM], light orange lines: O$_2$ flow per cell [amol·s^{-1}·x^{-1}] in DMSO control and dark orange lines: O$_2$ flow per cell [amol·s^{-1}·x^{-1}] in sunitinib-treated cells. "x" represents the unit cell. **(c, f)** O$_2$ flow (R, L, E) [amol·s^{-1}·x^{-1}] baseline-corrected for *Rox* in **(c)** RPMI^{+FBS} and **(f)** HPLM^{+FBS}. **(d, g)** Flux control ratios *FCR* in SW620 cells grown in **(d)** RPMI^{+FBS} and **(g)** HPLM^{+FBS} and exposed to sunitinib (chemical structure depicted) Median ± IQR (50 % range). 2-way ANOVA with Bonferroni´s multiple comparison test; *N*= 5 - 6.

Third, *R/E* and *L/E* ratios were elevated in cells grown in HPLM^{+FBS} and exposed to sunitinib as compared with DMSO (Figure 5g, Table S2b). Taken together, these results suggest that sunitinib exerts an inhibitory effect on the electron transfer system and additionally a partial dyscoupling effect as indicated by the increase of L and L/E. While dyscoupling reduces the efficiency of ATP production, this is in part compensated for by increasing ROUTINE respiration. These conclusions are corroborated by the drop of the *E-L* net ET capacity and *E-L* coupling efficiency in cells

exposed to sunitinib, whereas the net R/E control ratio was constant (Table S2b). The slight decrease in the R-L control efficiency $(R$-$L)/R$ (Table S2b) reflects a drop in the fraction of ROUTINE respiration coupled to phosphorylation, indicating that mitochondrial dyscoupling by sunitinib when cells are grown in HPLM[+FBS] was not fully compensated for by an increase of ROUTINE respiration (Hutter et al 2004; Gnaiger 2021; Zdrazilova et al 2022). Bioenergetic cluster analysis BCA extends these observations (Figure 6), showing two heterolinear clusters when LEAK respiration was expressed over ET with a cluster of cells grown in HPLM[+FBS] treated with sunitinib with higher L (Figure 6f). Furthermore, two clusters were detected with a drop in the coupling efficiency in cells grown in HPLM[+FBS] and treated with sunitinib (Figure 6h).
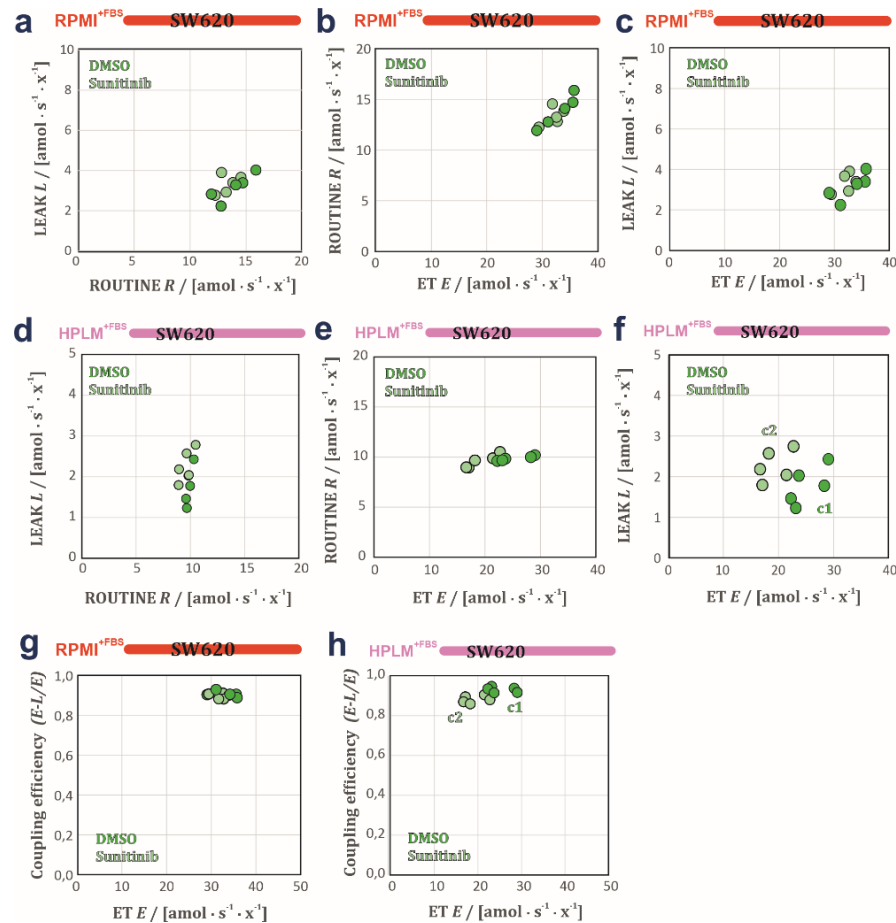

Figure 6. Bioenergetic cluster analysis in different respiratory coupling states of the SW620 cells grown in RPMI[+FBS] and HPLM[+FBS] media exposed to sunitinib. Plots of L over R, R over E, and L over E. **(a-c)** SW620 cells grown in RPMI[+FBS] and exposed either to DMSO or 10 μM sunitinib for 3h. No cluster differences between DMSO and sunitinib are observed. **(d-f)** SW620 cells grown in HPLM[+FBS] and exposed to either DMSO or 10 μM sunitinib for 3 h. In this case, two heterolinear clusters (c1, DMSO and c2, sunitinib) were detected when L is plotted over E, one with higher L when E is decreasing (c2) indicating dyscoupling induced by sunitinib. **(g-h)** Coupling efficiencies $(E$-$L)/E$ over ET capacities in SW620 cells grown in RPMI[+FBS] **(g)** and HPLM[+FBS] **(h)**, and exposed to either DMSO or 10 μM sunitinib for 3 h**.** The two clusters, one with lower $(E$-$L)/E$ values in cells grown in HPLM[+FBS] and exposed to sunitinib (c2) indicates a drop in mitochondrial quality with the sunitinib treatment (Gnaiger 2021; Zdrazilova et al 2022).

Finally, we present evidence that the cancer drug sunitinib causes mitochondrial dysfunction only in SW620 cells grown in HPLM, whereas this effect was masked in cells grown in a classical culture medium. In conclusion, drug efficacies and off-target effects are cell type-specific and dependent on the culture media composition.

4. Discussion

Cancer drug discovery in the preclinical phase starts in many cases with cell culture models. In the first-stage of cell-based drug evaluations cell culture experiments are initiated to determine lead molecule potencies, efficacies and the toxicity profile (Astashkina et al 2012, Gordon et al 2018, Larsson et al 2020, Mayrhofer et al 2020, Röck et al 2019). One major drawback of drug discovery is the subsequent translation to animal models which depend on the reliability of these preclinical evaluations. The lack of reproducibility and the discrepancies between *in vivo* and *in vitro* models is calling for better defined cell culture conditions especially for analyzing cancer pathophysiology. Recent studies demonstrate that the culture medium formulation significantly affects the results obtained in commonly used cell biology assays (i.e. colony formation, uridine metabolism, transcriptomics) (Cantor et al 2017; Grzes et al 2021; Leney-Greene et al 2020; Vande Voorde et al 2019).

In our study we evaluated more physiological cell culture conditions, deciphering the impact of the newly formulated HPLM on proliferation and cell respiration and in three standard human cancer cell lines. Moreover, we tested whether the effect of the FDA-approved multikinase inhibitor sunitinib on mitochondrial function is influenced by growth conditions in HPLM. First, HPLM supported cell growth of all cancer cell lines tested. Second, HPLM exerts in a cell-type specific manner diverse effects on cell proliferation when compared to the classical media. Our data are consistent with previous observations showing that physiological media formulation affects proliferation kinetics in cancer cells (Cantor et al 2017; Vande Voorde et al 2019). Third, HPLM altered the mitochondrial bioenergetic profiles in two of the three cell lines in a cell type-specific manner. Fourth, HPLM revealed a mitochondrial dysfunction produced by cells exposed to the cancer drug sunitinib which was not present in the respective cells grown in classical media.

Our results provide a fingerprint of bioenergetic profiles in living cells for analysis of the effects of HPLM in steady state and under treatment with kinase inhibitors. Cell respiration was improved in two of the three cell lines. However, cell respiration of cancer cell lines was differentially affected. In SW620 cells, respiratory rates were not affected but changes in coupling-control ratios related to ROUTINE respiration indicate that HPLM influences energy demand which correlates with lower proliferation rate in HPLM. In MCF7 and A375 cells, we observed an increase of ROUTINE respiration and ET capacity which was more pronounced in the melanoma cell line. In MCF7 cells, this enhancement related to a higher coupling efficiency results in a higher mitochondrial quality with HPLM. In A375 cells, HPLM increased respiration in all coupling control states, suggesting that HPLM enhanced mitochondrial biogenesis without alteration of coupling efficiency. Our respiratory studies do not exclude the possibility that HPLM might affect the aerobic glycolysis phenotype which is found in many cancer cell lines (Hosios et al 2016). This mechanism might be relevant in connection with our findings that sunitinib exerts a mitochondrial dyscoupling effect in SW620 when grown in HPLM. This would make the cells more sensitive to the drug due to the high dependence to the glucose metabolism

and glucose uptake observed in colon cancer cells (Brown et al 2018; Shen et al 2020). Our findings support previous observations that the cell environment dictates cancer drug sensitivity, e.g. for the mitochondrial drug metformin (Gui et al 2016; Meng et al 2021). This underlines the fact that off-target toxicity driven by drugs usually produces a mitochondrial dysfunction related to the coupling state (Bouitbir et al 2019; Nadanaciva et al 2009; Paech et al 2018).

The results presented in this work show that HPLM alters both the proliferative behavior and mitochondrial bioenergetic states of living cells when compared to classic cell culture media. These observations obtained with three highly proliferative cancer cell lines of different origin need to be considered in future studies related to molecular analyses and using intervention strategies versus cancer cell models. HPLM mimics a more physiological situation leading to differences in cell proliferation and cell respiration, which needs to be considered for drawing translational conclusions. Importantly, one FDA-approved drug impaired mitochondrial function depending on the media composition. This observation must be considered for interpretations of drug efficacies and their off-target effects. Further standardization of cell culture media will help to solve the current reproducibility crisis in cancer biology (Errington et al 2021) and, in general, in *in vitro* 2D cell models. Our study should increase the awareness of the importance of the cell culture set-up to better streamline the time and cost-intensive quest for identifying more effective lead molecules in preclinical cancer research.

Abbreviations

Ama	antimycin A	N	number of independent replicates
amol	attomole (10^{-18} mol)		
BCA	bioenergetic cluster analysis	Omy	oligomycin
CCCP	carbonyl cyanide 3-chlorophenylhydrazone	R and R'_{tot}	ROUTINE respiration, *Rox*-corrected and total
E and E'_{tot}	electron transfer capacity *Rox*-corrected and total	Rot	rotenone
		ROX	residual oxygen consumption state
HPLM	Human Plasma-like Media		
FBS	Fetal bovine serum	*Rox*	residual O_2 consumption rate
FCR	flux control ratio	SUIT	Substrate-Uncoupler-Inhibitor-Titration
HRR	high-resolution respirometry		
I_{O_2}	O_2 flow per cell [amol·s^{-1}·x^{-1}]	U	Uncoupler
L and L'_{tot}	LEAK respiration, *Rox*-corrected and total	x	elementary unit

Acknowledgements

References

Astashkina A, Mann B, Grainger DW (2012) A critical evaluation of in vitro cell culture models for high-throughput drug screening and toxicity. Pharmacol Ther 134:82-106. https://doi.org/10.1016/j.pharmthera.2012.01.001

Bouitbir J, Alshaikhali A, Panajatovic MV, Abegg VF, Paech F, Krahenbuhl S (2019) Mitochondrial oxidative stress plays a critical role in the cardiotoxicity of sunitinib: Running title: Sunitinib and oxidative stress in hearts. Toxicology 426:152281. https://doi.org/10.1016/j.tox.2019.152281

Brown RE, Short SP, Williams CS (2018) Colorectal Cancer and Metabolism. Curr Colorectal Cancer Rep 14:226-241. https://doi.org/10.1007/s11888-018-0420-y

Cantor JR, Abu-Remaileh M, Kanarek N, Freinkman E, Gao X, Louissaint A Jr., Lewis CA, Sabatini DM (2017) Physiologic Medium Rewires Cellular Metabolism and Reveals Uric Acid as an Endogenous Inhibitor of UMP Synthase. Cell 169:258-272 e17. https://doi.org/10.1016/j.cell.2017.03.023

Chiusa M, Hool SL, Truetsch P, Djafarzadeh S, Jakob SM, Seifriz F, Scherer SJ, Suter TM, Zuppinger C, Zbinden S (2012) Cancer therapy modulates VEGF signaling and viability in adult rat cardiac microvascular endothelial cells and cardiomyocytes. J Mol Cell Cardiol 52:1164-75. https://doi.org/10.1016/j.yjmcc.2012.01.022

Doerrier C, Garcia-Souza LF, Krumschnabel G, Wohlfarter Y, Meszaros AT, Gnaiger E (2018) High-Resolution FluoRespirometry and OXPHOS Protocols for Human Cells, Permeabilized Fibers from Small Biopsies of Muscle, and Isolated Mitochondria. Methods Mol Biol 1782:31-70. https://doi.org/10.1007/978-1-4939-7831-1_3

Eagle H (1955) Nutrition needs of mammalian cells in tissue culture. Science 122:501-14. https://doi.org/10.1126/science.122.3168.501

Eagle H (1959) Amino acid metabolism in mammalian cell cultures. Science 130:432-7. https://doi.org/10.1126/science.130.3373.432

Gnaiger E (2020) Mitochondrial pathways and respiratory control. An introduction to OXPHOS analysis. 5th ed. Bioenerg Commun 2020.2. https://doi.org/doi:10.26124/bec:2020-0002

Gnaiger E (2021) Bioenergetic cluster analysis – mitochondrial respiratory control in human fibroblasts. Mitofit Preprints 2021.8. https://doi.org/doi:10.26124/mitofit:2021-0008

Goodman VL, Rock EP, Dagher R, Ramchandani RP, Abraham S, Gobburu JV, Booth BP, Verbois SL, Morse DE, Liang CY, Chidambaram N, Jiang JX, Tang S, Mahjoob K, Justice R, Pazdur R (2007) Approval summary: sunitinib for the treatment of imatinib refractory or intolerant gastrointestinal stromal tumors and advanced renal cell carcinoma. Clin Cancer Res 13:1367-73. https://doi.org/10.1158/1078-0432.CCR-06-2328

Gordon JL, Brown MA, Reynolds MM (2018) Cell-Based Methods for Determination of Efficacy for Candidate Therapeutics in the Clinical Management of Cancer. Diseases 6:85. https://doi.org/10.3390/diseases6040085

Grzes KM, Sanin DE, Kabat AM, Stanczak MA, Edwards-Hicks J, Matsushita M, Hackl A, Hässler F, Knoke K, Zahalka S, Villa M, Kofler DM, Voll RE, Zigrino P, Fabri M, Pearce EL, Pearce EJ (2021) Plasmacytoid dendritic cell activation is dependent on coordinated expression of distinct amino acid transporters. Immunity 54:2514-2530 e7. https://doi.org/10.1016/j.immuni.2021.10.009

Gui DY, Sullivan LB, Luengo A, Hosios AM, Bush LN, Gitego N, Davidson SM, Freinkman E, Thomas CJ, Vander Heiden MG (2016) Environment Dictates Dependence on Mitochondrial Complex I for NAD+ and Aspartate Production and Determines Cancer Cell Sensitivity to Metformin. Cell Metab 24:716-727. https://doi.org/10.1016/j.cmet.2016.09.006

Hosios AM, Hecht VC, Danai LV, Johnson MO, Rathmell JC, Steinhauser ML, Manalis SR, Vander Heiden MG (2016) Amino Acids Rather than Glucose Account for the Majority of Cell Mass in Proliferating Mammalian Cells. Dev Cell 36:540-9. https://doi.org/10.1016/j.devcel.2016.02.012

Hutter E, Renner K, Pfister G, Stockl P, Jansen-Durr P, Gnaiger E (2004) Senescence-associated changes in respiration and oxidative phosphorylation in primary human fibroblasts. Biochem J 380:919-28. https://doi.org/10.1042/BJ20040095

Kapalczynska M, Kolenda T, Przybyla W, Zajaczkowska M, Teresiak A, Filas V, Ibbs M, Blizniak R, Luczewski L, Lamperska K (2018) 2D and 3D cell cultures - a comparison of different types of cancer cell cultures. Arch Med Sci 14:910-919. https://doi.org/10.5114/aoms.2016.63743

Larsson P, Engqvist H, Biermann J, Werner Ronnerman E, Forssell-Aronsson E, Kovacs A, Karlsson P, Helou K, Parris TZ (2020) Optimization of cell viability assays to improve replicability and reproducibility of cancer drug sensitivity screens. Sci Rep 10:5798. https://doi.org/10.1038/s41598-020-62848-5

Leney-Greene MA, Boddapati AK, Su HC, Cantor JR, Lenardo MJ (2020) Human Plasma-like Medium Improves T Lymphocyte Activation. iScience 23:100759. https://doi.org/10.1016/j.isci.2019.100759

Mayrhofer JE, Enzler F, Feichtner A, Röck R, Fleischmann J, Raffeiner A, Tschaikner P, Ogris E, Huber RG, Hartl M, Schneider R, Troppmair J, Torres-Quesada O, Stefan E (2020) Mutation-oriented profiling of autoinhibitory kinase conformations predicts RAF inhibitor efficacies. Proc Natl Acad Sci U S A 117:31105-31113. https://doi.org/10.1073/pnas.2012150117

Meng L, Chen D, Meng G, Lu L, Han C (2021) Dysregulation of the Sirt5/IDH2 axis contributes to sunitinib resistance in human renal cancer cells. FEBS Open Bio 11:921-931. https://doi.org/10.1002/2211-5463.13090

Moore GE, Gerner RE, Franklin HA (1967) Culture of normal human leukocytes. JAMA 199:519-24.

Moreno-Sanchez R, Saavedra E, Rodriguez-Enriquez S, Gallardo-Perez JC, Quezada H, Westerhoff HV (2010) Metabolic control analysis indicates a change of strategy in the treatment of cancer. Mitochondrion 10:626-39. https://doi.org/10.1016/j.mito.2010.06.002

Moretto J, Chauffert B, Ghiringhelli F, Aldrich-Wright JR, Bouyer F (2011) Discrepancy between in vitro and in vivo antitumor effect of a new platinum(II) metallointercalator. Invest New Drugs 29:1164-76. https://doi.org/10.1007/s10637-010-9461-z

Morgan JF, Morton HJ, Parker RC (1950) Nutrition of animal cells in tissue culture; initial studies on a synthetic medium. Proc Soc Exp Biol Med 73:1-8. https://doi.org/10.3181/00379727-73-17557

Nadanaciva S, Will Y (2009) Current concepts in drug-induced mitochondrial toxicity. Curr Protoc Toxicol Chapter 2: Unit 2 15. https://doi.org/10.1002/0471140856.tx0215s40

Paech F, Abegg VF, Duthaler U, Terracciano L, Bouitbir J, Krahenbuhl S (2018) Sunitinib induces hepatocyte mitochondrial damage and apoptosis in mice. Toxicology 409:13-23. https://doi.org/10.1016/j.tox.2018.07.009

Parri M, Ippolito L, Cirri P, Ramazzotti M, Chiarugi P (2020) Metabolic cell communication within tumour microenvironment: models, methods and perspectives. Curr Opin Biotechnol 63:210-219. https://doi.org/10.1016/j.copbio.2020.03.001

Rinaldi L, Delle Donne R, Borzacchiello D, Insabato L, Feliciello A (2018) The role of compartmentalized signaling pathways in the control of mitochondrial activities in cancer cells. Biochim Biophys Acta Rev Cancer 1869:293-302. https://doi.org/10.1016/j.bbcan.2018.04.004

Röck R, Mayrhofer JE, Torres-Quesada O, Enzler F, Raffeiner A, Raffeiner P, Feichtner A, Huber RG, Koide S, Taylor SS, Troppmair J, Stefan E (2019) BRAF inhibitors promote intermediate BRAF(V600E) conformations and binary interactions with activated RAS. Science Advances 5:eaav8463. https://doi.org/10.1126/sciadv.aav8463

Rossiter NJ, Huggler KS, Adelmann CH, Keys HR, Soens RW, Sabatini DM, Cantor JR (2021) CRISPR screens in physiologic medium reveal conditionally essential genes in human cells. Cell Metab 33:1248-1263 e9. https://doi.org/10.1016/j.cmet.2021.02.005

Sams-Dodd F (2005) Target-based drug discovery: is something wrong? Drug Discov Today 10:139-47. https://doi.org/10.1016/S1359-6446(04)03316-1

Schopf B, Schafer G, Weber A, Talasz H, Eder IE, Klocker H, Gnaiger E (2016) Oxidative phosphorylation and mitochondrial function differ between human prostate tissue and cultured cells. The FEBS journal 283:2181-96. https://doi.org/10.1111/febs.13733

Shen C et al. (2020) m(6)A-dependent glycolysis enhances colorectal cancer progression. Mol Cancer 19:72. https://doi.org/10.1186/s12943-020-01190-w

Vande Voorde J, Ackermann T, Pfetzer N, Sumpton D, Mackay G, Kalna G, Nixon C, Blyth K, Gottlieb E, Tardito S (2019) Improving the metabolic fidelity of cancer models with a physiological cell culture medium. Sci Adv 5:eaau7314. https://doi.org/10.1126/sciadv.aau7314

Zdrazilova L, Hansikova H, Gnaiger E (2022) Comparable respiratory activity in attached and suspended human fibroblasts. PLoS One 17:e0264496. https://doi.org/10.1371/journal.pone.0264496
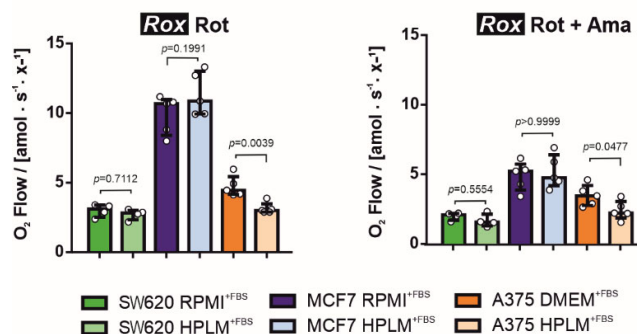
Supplement

Figure S1. Differences on ROX between classical and HPLM media in SW620, MCF7, and A375 cell populations. Comparison of residual O_2 consumption (*Rox*) after rotenone (Rot, left panel) and rotenone + antimycin A additions (Rot + Ama, right panel) in SW620, MCF7 and A375 cell lines grown in RPMI^{+FBS} / DMEM^{+FBS} and HPLM^{+FBS}. Values of O_2 flow [amol·s^{-1}·x^{-1}] are represented as median ± IQR (50 % range). 2-wayANOVA with Bonferroni´s multiple comparison test; *N* = 4.

Table S1. Respiration of cancer cell lines SW620, MCF7, and A375 in classical media (RPMI+FBS or DMEM+FBS) and HPLM+FBS. Median ± IQR (50 % range). **(a)** *R, L* and *E* corrected for residual oxygen consumption *Rox*. *N* are biological replicates. **(b)** Flux control ratios, net capacities and flux control efficiencies normalized for ROUTINE or ET capacity as an internal normalization to express respiration independent of cell count. *Rox/E′tot* ratio is *Rox* normalized against the total *E′tot*. *E′tot* is the ET capacity without *Rox* correction. Bold case indicates statistical significance at *p≤0.05.*

a	Cell line - culture media	Number of repeats *N* or groups	ROUTINE *R* [amol·s⁻¹·x⁻¹]	LEAK *L* [amol·s⁻¹·x⁻¹]	ET capacity *E* [amol·s⁻¹·x⁻¹]	*Rox* [amol·s⁻¹·x⁻¹]
	SW620-RPMI+FBS	*N = 4*	24.39 ± 4.82	5.86 ± 0.66	62.83 ± 9.13	1.90 ± 0.26
	SW620-HPLM+FBS	*N = 4*	24.95 ± 0.88	5.14 ± 0.31	60.13 ± 2.48	1.55 ± 0.32
	MCF7-RPMI+FBS	*N = 5*	79.31 ± 4.78	30.79 ± 3.95	**180.90 ± 14.03**	5.22 ± 1.01
	MCF7-HPLM+FBS	*N = 5*	94.95 ± 2.67	28.85 ± 11.96	**218.51 ± 3.62**	4.74 ± 1.38
	A375-RPMI+FBS	*N = 5*	**20.16 ± 0.79**	6.12 ± 0.28	**57.73 ± 9.71**	**3.44 ± 0.90**
	A375-HPLM+FBS	*N = 5*	**35.06 ± 3.13**	8.83 ± 1.85	**92.22 ± 6.05**	**2.21 ± 0.51**

b	Cell line - culture media	Number of repeats *N* or groups	control ratio *R/E*	control ratio *L/E*	control ratio *L/R*	net ET capacity *E-L* [amol·s⁻¹·x⁻¹]	net *R/E* ratio (R-L)/E	*E-L* coupling efficiency (E-L)/E	*R-L* control efficiency (R-L)/R	ROX *Rox / E′tot*
	SW620-RPMI+FBS	*N = 4*	**0.40 ± 0.01**	0.10 ± 0.01	**0.25 ± 0.03**	56,51± 7.23	**0.30 ± 0.02**	0.90 ± 0.01	**0.75 ± 0.03**	0,03 ± 0.00
	SW620-HPLM+FBS	*N = 4*	**0.42 ± 0.02**	0.09 ± 0.01	**0.21 ± 0.01**	54.52 ± 2.26	**0.33 ± 0.01**	0.91 ± 0.01	**0.79 ± 0.01**	0,03 ± 0.01
	MCF7-RPMI+FBS	*N = 5*	0.45 ± 0.02	**0.16 ± 0.04**	0.37 ± 0.06	**154.42 ± 16.10**	0.28 ± 0.01	0.84 ± 0.04	0.63 ± 0.06	0,03 ± 0.01
	MCF7-HPLM+FBS	*N = 5*	0.43 ± 0.01	**0.13 ± 0.06**	0.31 ± 0.12	**181.91 ± 5.57**	0.30 ± 0.04	0.87 ± 0.06	0.69 ± 0.12	0,02 ± 0.01
	A375-RPMI+FBS	*N = 5*	0.35 ± 0.03	0.10 ± 0.00	0.30 ± 0.02	**51.45 ± 9.58**	0.25 ± 0.03	0.90 ± 0.00	0.70 ± 0.02	**0,06 ± 0.00**
	A375-HPLM+FBS	*N = 5*	0.37 ± 0.01	0.09 ± 0.01	0.25 ± 0.03	**81.44 ± 5.55**	0.27 ± 0.00	0.91 ± 0.01	0.75 ± 0.03	**0,03 ± 0.01**

Table S2. Sunitinib effect on SW620 cell respiration in RPMI+FBS and HPLM+FBS. Median ± IQR (50 % range). **(a)** *R*, *L* and *E* corrected for residual oxygen consumption *Rox*. *N* are biological replicates. **(b)** Flux control ratios, net capacities and flux control efficiencies normalized for ROUTINE or ET capacity as an internal normalization to express respiration independent of cell count. Bold font indicates statistical significance at *p≤0.05* using a non-parametric unpaired t-test.

a

Cell line - culture media		Number of repeats N or groups	ROUTINE R [amol·s⁻¹·x⁻¹]	LEAK L [amol·s⁻¹·x⁻¹]	ET capacity E [amol·s⁻¹·x⁻¹]	Rox [amol·s⁻¹·x⁻¹]
SW620-RPMI+FBS	DMSO	N = 6	13.11 ± 3.74	2.90 ± 1.47	31.58 ± 7.92	0.76 ± 0.44
	Sunitinib	N = 6	13.23 ± 1.42	3.26 ± 0.84	32.23 ± 1.79	0.66 ± 0.40
SW620-HPLM+FBS	DMSO	N = 5	9.86 ± 0.45	1.79 ± 0.88	**25.30 ± 5.97**	0.98 ± 0.15
	Sunitinib	N = 5	9.59 ± 1.23	2.27 ± 0.74	**19.24 ± 5.22**	0.98 ± 0.27

b

Cell line - culture media		Number of repeats N or groups	control ratio R/E	control ratio L/E	control ratio L/R	net ET capacity E-L [amol·s⁻¹·x⁻¹]	net R/E ratio (R-L)/E	E-L coupling efficiency (E-L)/E	R-L control efficiency (R-L)/R
SW620-RPMI+FBS	DMSO	N = 6	0.41 ± 0.02	0.09 ± 0.03	0.22 ± 0.07	28.68 ± 6.69	0.32 ± 0.02	0.91 ± 0.03	0.78 ± 0.07
	Sunitinib	N = 6	0.41 ± 0.04	0.10 ± 0.03	0.25 ± 0.04	28.97 ± 2.11	0.31 ± 0.03	0.90 ± 0.03	0.75 ± 0.04
SW620-HPLM+FBS	DMSO	N = 5	**0.39 ± 0.07**	**0.07 ± 0.03**	0.18 ± 0.08	**23.51 ± 5.34**	0.32 ± 0.09	**0.93 ± 0.03**	**0.82 ± 0.08**
	Sunitinib	N = 5	**0.50 ± 0.07**	**0.12 ± 0.04**	0.24 ± 0.06	**16.97 ± 4.81**	0.34 ± 0.06	**0.88 ± 0.04**	**0.76 ± 0.06**